Analytic model of a two-wire thermal sensor for flow and sound measurements

J W van Honschoten, G J M Krijnen, V B Svetovoy, H-E de Bree and M C Elwenspoek

Transducers Science and Technology Group, MESA+ Research Institute,
University of Twente, PO 217, 7500 AE Enschede, The Netherlands

E-mail: j.w.vanhonschoten@el.utwente.nl

Abstract
The Microflown is an acoustic sensor that measures particle velocity instead of pressure, as conventional microphones do. This paper presents an analytical model describing the physical processes that govern the behaviour of the sensor and determine its sensitivity. Forced convection by an acoustic wave causes a small, asymmetrical, perturbation to the temperature profile around the two heated wires of the sensor, so that a temperature difference between these wires occurs. This temperature difference, to which the sensitivity is proportional, is calculated with a perturbation theory. Subsequently the frequency-dependent behaviour of the sensitivity can be analysed; it is found that there are two important corner frequencies, the first related to the time constant of heat diffusion, and the second related to the heat capacity of the heaters.

A thorough description has already been given for the realization of the Microflown in a channel, i.e. with fixed walls acting as heat sinks near both heaters. Here, an analytic and two-dimensional model is presented that describes the situation of the present sensor without walls above and under it. Contrary to the previous model, this analytic model allows easy understanding of the sensor and is especially useful for engineering purposes due to its relative simplicity. Especially for small wire separations, the developed analysis appears to be in good agreement with experimental results and the model therefore offers the possibility of optimizing the sensor.

1. Introduction

The Microflown is an acoustic sensor based on a thermal principle [1]. Since its invention in 1994 [2], it has mostly been used for measurement purposes (1D and 3D-sound intensity measurement [3–6], acoustic impedance [7, 8] and pressure [9]). The Microflown is also used as an add-on microphone for professional recording purposes [14]. This is because the Microflown is, in contrast to pressure gradient microphones, comparatively sensitive to low frequency sound waves. A particle velocity sensor with a wide measurable frequency spectrum can be obtained by a combination of a Microflown and a so-called 'pressure gradient' microphone and has a 'figure-of-eight' polar pattern of sensitivity. The Microflown is also used for measuring dc flows [10], and can be used as a

mass flow sensor [17–19]. Sound-energy determination with this sensor is under investigation.

The Microflown consists of two closely spaced (ca 100 μm) thin wires of silicon nitride, similar to [16], with an electrically conducting platinum pattern on top of them. Dimensions of the two wires are $1000 \times 2 \times 0.3$ μm ($l \times w \times h$). The metal pattern is used as a heater *and* as a temperature sensor, by using its temperature-dependent resistance. The silicon nitride layer is used as a mechanical support for the platinum resistor patterns. The sensors are powered by an electrical current, and heated to an operational temperature between 200 °C and 500 °C.

When a particle velocity is present, the temperature distribution around the resistors is asymmetrically altered, and a temperature difference between the two wires occurs. In a
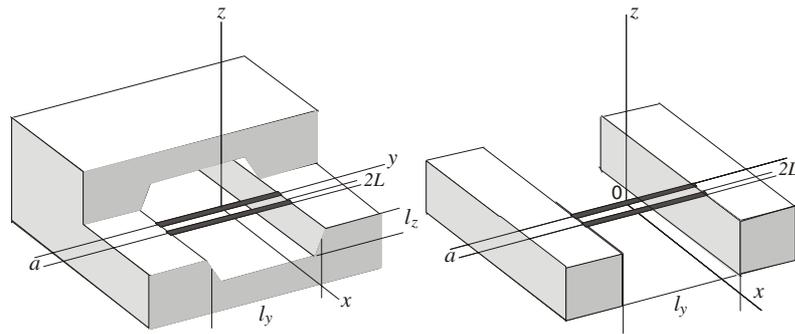
Figure 1. Geometry of the sensor used in the analysis. Left: geometry used in the previous model [12]; right: geometry analysed in this paper, without walls above and under the heaters.

first-order approximation, this temperature difference of the two wires is proportional to the particle velocity, and since the resistance of the heated wires increases with their temperature, it can be electronically measured. Due to heat diffusion effects in the fluid and the thermal mass of the wires, the thermal response of the wires decreases with increasing frequencies. The Microflown therefore exhibits a decrease in sensitivity with increasing frequencies.

2. A physical model of the temperature distribution around the Microflown

A detailed three-dimensional model of the device was developed a few years ago [12]. In that model, a final expression for the sensitivity was obtained by calculating a multiple sum of a definite function. Though the sums converge rather fast, the result is not very convenient for engineers designing the Microflown for a specific application. Significant progress achieved in the Microflown technology since then offers the possibility of simplifying the model. First, the wire width was reduced to 2 μm and its thickness became 100 nm for the platinum layer and 200 nm for the silicon nitride support. These sizes are much smaller than all the other dimensions. Therefore, in most cases one can consider the wire as a one-dimensional object except for the situations in which the width or thickness of the wire plays an essential role. Second, the technology has allowed making the wires longer so that a two-dimensional approach is a good approximation for real devices. Third, in many cases the surrounding surfaces are at a distance from the wires that is large compared to their mutual distance, so that one can consider them as free standing.

Our aim here is to get a relatively simple explicit expression for the sensor sensitivity, which has a sufficient precision for, and is thus very useful for, engineering applications. The model to be constructed is two-dimensional, analytic and also permits a better understanding of the behaviour of the sensor.

In this model, the Microflown consists of two infinitely long heaters of width L and thickness h, separated by a distance a, which is much larger than L or h. We will neglect the transverse wire dimensions everywhere where it does not bring any physical contradictions. For example, the heater temperature will be diverging in the $L \to 0$ limit. In this case a simple way to take into account the finite wire width will

be proposed. The wire width and thickness are also important when the effect of the thermal mass of the wire is considered.

A certain particle velocity with amplitude v is assumed as the signal to be measured. Although it can be expected that the wires slightly influence the velocity profile around them, the measured velocity v near the wires is supposed to be proportional to the particle velocity. It is a matter of convention because generally the sensor has to be calibrated due to a more significant influence of the package gain.

It should be stressed that the device is operating at velocities very small in comparison with that typical for hot wire anemometry. The Microflown is able to measure particle velocities as small as 50 nm s^{-1} [23]. A sound pressure of 1 Pa (94 dB) corresponds to a velocity $v = 2.2$ mm s^{-1}, while anemometers lose their sensitivity at velocities of about $v \sim 1$ cm s^{-1} [15, 21, 24].

The signal of the sensor, that is the output voltage u_0, is proportional to the temperature difference ΔT between the wires due to a particle velocity, according to [1, 12]

$$u_0 = \frac{U_0}{2}\theta \Delta T(v), \tag{1}$$

where U_0 is the applied voltage over the sensor wires and θ is the temperature coefficient of the resistance. Thus, an expression for ΔT has to be found.

The heated wires cause a temperature distribution of the air around them. This undisturbed temperature profile, not yet influenced by an acoustical wave, is calculated first. Subsequently, this profile is used as a starting point for the calculation of the temperature difference of the heaters that occurs when a flow is applied, by addition of a perturbation to the original temperature profile.

In section 2.1, the stationary temperature distribution is calculated, so that in section 2.2 the influence of an acoustic wave can be analysed as a perturbation to this function, and in section 2.3 the effect of the finite heat capacity of the sensors on the frequency behaviour is taken into account.

2.1. The stationary situation

The temperature profile around the heaters in the two-wire realization of the Microflown is adequately described in [12] for the configuration of the channel with fixed walls in the positive and negative y, z-directions (see figure 1). In this paper, a configuration is assumed in which no walls in the y- or z-direction are present, and a theory is developed to find an

analytical expression for the temperature difference between the wires and so for the sensitivity of the sensor.

The stationary heat transport equation for this geometry reads

$$-\nabla(k\nabla T) = Q, \qquad (2)$$

where $k = k(T)$ represents the heat conductivity of the medium, and Q is the amount of heat generated per unit time and volume. Suppose first that the heater is infinitely long in the y-direction (l_y much larger than all other dimensions) and infinitely thin in the x- and z-directions. Since the total power is P and the power per unit of length is P/l_y for the heat source one can write

$$Q = \frac{P}{l_y}\delta(x)\delta(z), \qquad (3)$$

where the δ-functions appear at the heater position. It was shown in [12] that the heat flux through the beam ends to the substrate is small compared to the total dissipated power. Therefore, the parts of the heater at the ends where a temperature gradient occurs are short compared to the total wire length, and the temperature in the middle can be considered to be constant over a relatively long distance. The problem is thus reduced to a two-dimensional one and therefore becomes simpler than the model based on the expansion in harmonics of [12]. Additionally, we will assume that k is independent of T. For high wire temperatures (400–500 °C), this assumption is true with a precision of about 10%. This can be considered as an acceptable precision for engineering purposes. In this case equation (2) is simplified as

$$\left(\partial_x^2 + \partial_z^2\right)T = -\frac{P}{l_y k}\delta(x)\delta(z). \qquad (4)$$

The general solution of this equation is

$$T(r) = -\frac{P}{2\pi k l_y}\ln\frac{r}{r_0}, \qquad r = \sqrt{x^2 + z^2}, \qquad (5)$$

where r_0 is an arbitrary constant. We are looking for the solution that is finite in the origin $x = y = 0$ and goes to zero at infinity. Obviously (4) shows divergences in both these limits. The divergence in the origin has a clear physical meaning; we did not take into account the finite width of the wire. It can be easily taken into consideration in the way described below. The divergence at infinity reflects the two-dimensional nature of the problem; there is no physical system that is exactly two dimensional. At large distances, the logarithmic behaviour should be changed due to the finite length of the wire. The question is to what extent we can use solution (5) and what is the value of r_0.

The answer is that equation (5) describes the behaviour of a real three-dimensional system with so-called logarithmic precision. Let us first note that the arbitrary constant r_0 has to be proportional to the only length scale l_y (current Microflowns have a wire length of 1500 μm). Then the logarithmic precision means that our solution is true while

$$\left|\ln\left(\frac{r}{l_y}\right)\right| \gg 1. \qquad (6)$$

We are interested in the temperature distribution on distances of the order of 100 μm (separation between the wires), therefore, the logarithmic precision is only 40%. This is not

too good. Fortunately there is a possibility of improving the solution accuracy.

One can find the exact solution of the three-dimensional problem with the geometry shown in figure 1 (right) and see how it can be approximated by equation (5). The three-dimensional problem with the cold walls at $y = \pm l_y/2$ can be solved in a way similar to that described in [12]. We are looking for a solution as an expansion in harmonics

$$T(x, y, z) = \sum_{n=0}^{\infty} T_n(x, z)\cos(2\lambda_n y/l_y),$$

$$\lambda_n = \frac{\pi}{2}(2n + 1). \qquad (7)$$

In this way, the boundary conditions on the walls will be satisfied (for a physical discussion see [12]). For the amplitudes $T_n(x, z)$, we will find an equation similar to (4) but with an additional term

$$\left(\partial_x^2 + \partial_z^2\right)T_n - \left(\frac{2\lambda_n}{l_y}\right)^2 T_n = -\frac{2(-1)^n}{\lambda_n}\frac{P}{l_y k}\delta(x)\delta(z). \qquad (8)$$

It can be solved by making a two-dimensional Fourier transform to find

$$T_n(r) = \frac{P}{2\pi k l_y}\frac{2(-1)^n}{\lambda_n}K_0\left(\frac{2\lambda_n r}{l_y}\right), \qquad (9)$$

where $K_0(x)$ is the modified Bessel function of the second kind. It can be substituted in equation (7) to get the three-dimensional temperature distribution. This distribution is rather flat in the y-direction changing only near the walls [12]. In the limit $r \to 0$ it behaves as

$$T(x, 0, z) = -\frac{P}{2\pi k l_y}\left(\ln(r/l_y) - \gamma - 2\ln\Gamma(3/4) + \frac{3}{2}\ln\pi\right), \qquad (10)$$

where $\gamma = 0.577$ is the Euler constant and $\Gamma(x)$ is the gamma function. The function (10) behaves exactly as the solution of the two-dimensional problem (5) with the only difference that the constant r_0 has a definite value: $r_0/l_y = 0.480$. Comparison of the temperature distributions given by the exact solution of the three-dimensional problem (7) and (9), and that given by equation (5) is presented in figure 2 by the solid and dashed lines. One sees that the approximation is very good up to $r/l_y \leqslant 0.2$. This distance range covers all practical needs.

This is the most important conclusion from the above analysis because, as we will see later, for the calculation of the Microflown sensitivity we have to know the gradient of the stationary temperature distribution but not the temperature itself. However, this gradient does not depend on the parameter r_0 at all.

We justified the use of the two-dimensional solution and indicated the upper limit on the distance from the wire where the two-dimensional approximation is still applicable. Now let us discuss the divergence at $r \to 0$. Due to this divergence, equation (5) does not allow us to calculate the temperature of the wire itself. This is since we neglected the wire width. One can easily take into account the finite width of the wire in the following way. We can distribute the point-like sources in the x-direction on the wire in such a way that the boundary condition is fulfilled: the temperature on the wire is constant. It gives an integral equation for the source distribution function.
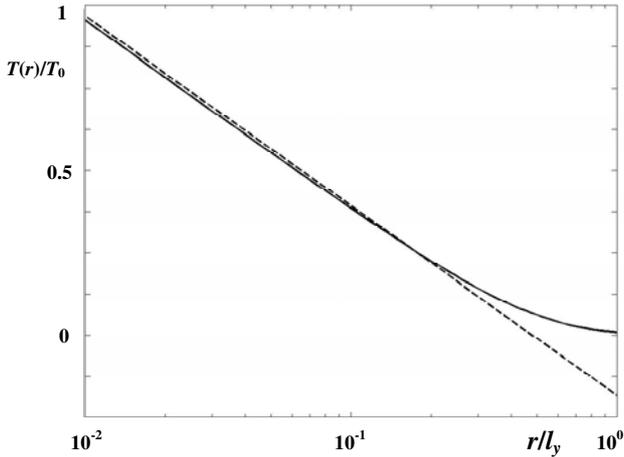
Figure 2. The temperature distribution given by the exact solution of the three-dimensional problem, equations (7) and (9) (solid line), compared to the approximation of equation (5) (dashed line).

However, since the wire is narrow, there is a much simpler approximate way. For a narrow wire, any distribution can be changed for the averaged one over the wire width. This approximation will be good while the temperature change on the wire is small in comparison with the temperature itself. For the wires as narrow as 2 μm, it is obviously the case. In mathematical language, this physical picture can be formulated as

$$ T(x, z) = -\frac{P}{2\pi k l_y} \frac{1}{2L} \int_{-L}^{L} \ln \frac{\sqrt{(x-x')^2 + z^2}}{r_0} \, dx'. \quad (11) $$

At distances much larger than the wire width, $|x|, |z| \gg L$, it coincides with (5), but on the wire itself it gives a finite temperature

$$ T(0, 0) = -\frac{P}{2\pi k l_y} (\ln(L/r_0) - 1). \quad (12) $$

The temperature distribution will be used as the basic one for the following. The integral in (11) can be found explicitly but it is not very informative since the point of interest is the temperature gradient but not the temperature itself. So we leave the integral in its original form for a while. During the calculation of the above temperature profile, only one heater was considered, see equation (4). Due to the linearity of the heat equation the solution for T is a sum of two solutions, one for a source at $x = 0$, and the other for a source at $x = a$. The new solution for T is therefore not fundamentally different from equation (4). It can be written, for example, in the form

$$ T_{\text{total}}(x) = T_{\text{left heater}}(x) + T_{\text{right heater}}(x), $$

where

$$ T_{\text{right heater}}(x) = T(x - a) \qquad \text{and} \qquad T_{\text{left heater}}(x) = T(x), $$

For two heaters at a mutual distance of 100 μm, a length l_y of 1.5 mm and a dissipated power of 10 mW, the temperature profile is shown in figure 3. On the scale of the figure, no difference can be distinguished between the exact solution (equations (7) and (9)) and the two-dimensional approximation.
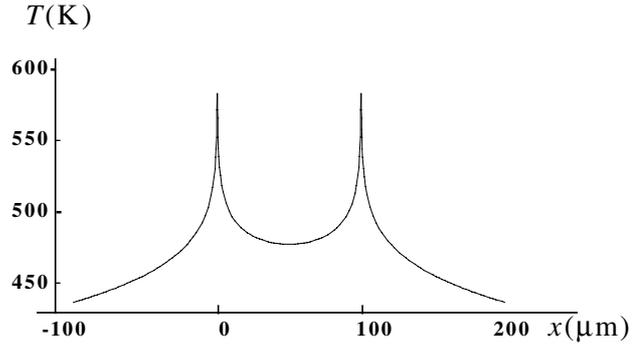

Figure 3. Temperature distribution around the two sensors in a stationary situation. The heaters are located at $x = 0$ and $x = 100$ μm, the dissipated power is approximately 10 mW.

2.2. Influence of an acoustic wave on the temperature profile

If the gas in the channel is moving, the temperature can be found from the heat equation

$$ \rho c_p (\partial_t T + \mathbf{v} \nabla T) - k \nabla^2 T = Q, \quad (13) $$

where $\mathbf{v}$ is the gas velocity, ρ and c_p are the density and heat capacity of the gas, respectively, and Q is the heat power density defined as before by equation (3). The convective term $\mathbf{v} \nabla T$ is responsible for the differential signal from the device that is the main concern of this paper.

The free convection is not significant in our case. Free convection is important in situations where the Grashof number Gr is larger than 1000 [25][1]. The operating temperatures of the Microflown are roughly 500 °C and its characteristic length is about 200 μm so that Gr $\ll$ 1 and the effect of free convection is only small. Any finite heat loss of the wires due to free convection and the related decrease in the efficiency can thus be only relatively small compared to the total power dissipation, and it can be assumed that the influence on the temperature profile is insignificant. Moreover, free convection will only cause stationary temperature differences between the wires, which only contribute an unimportant dc signal.

Let us consider two competing processes: the heat diffusion defined by the heat diffusion coefficient $D = k/\rho c_p \approx 1.9 \times 10^{-5}$ m^2 s^{-1} (air) and the forced convection defined by the velocity magnitude $v = 4.4$ mm s^{-1} (it corresponds to a very high acoustic pressure of 100 dB). Due to the diffusion the time to travel for a particle from one wire to the other is l^2/D; due to the forced convection this time will be l/v. Comparing these times yields

$$ \frac{v}{D/l} \ll 1, \quad (14) $$

because the diffusion velocity $D/l \approx 0.2$ m s^{-1} is large in comparison with v. This means that the temperature profile due to the heat conductivity is formed comparatively fast; the contribution of the convection is small so that

[1] The Grashof number is defined as

$$ \text{Gr} = \frac{g\beta \Delta T l^3}{\nu^2}, $$

where g is the gravity acceleration, β is the gas thermal expansion coefficient, ν is the kinematic viscosity, ΔT is the temperature change and l is a characteristic length.

the convective term in equation (13) can be treated as a perturbation. Therefore, we can consider the temperature as $T + \delta T$, where the first term is the temperature in still air that was found in the previous section and δT is the temperature correction caused by convection. For this correction one finds from (13) the following equation:

$$\partial_t \delta T - D\nabla^2 \delta T = -v\partial_x T, \qquad (15)$$

where it is assumed explicitly that the gas is moving only in the x-direction $\mathbf{v} = (v, 0, 0)$. First, we will consider the case of one heater. Generalization to the case of two heaters is straightforward since the equation is linear. On the right-hand side we have to substitute the temperature distribution for the stationary problem (11). It was already noted that the gradient $\partial_x T$ does not depend on the parameter r_0. Equation (15) has to be solved at the boundary condition $\delta T \rightarrow 0$ at large distances from the wires.

In acoustic applications we are interested in periodic signals, therefore, we will consider the particle velocity in the sound wave in the harmonic form $v = v_0 \exp(\mathrm{i}2\pi f t)$ with a frequency f. The temperature correction is then also harmonic in time $\delta T = \delta T(x, z) \exp(\mathrm{i}2\pi f t)$ with the amplitude $\delta T(x, z)$ depending only on the coordinates. This amplitude can be found from the equation

$$\mathrm{i}2\pi f \delta T - D(\partial_x^2 + \partial_z^2)\delta T = -v_0 \partial_x T, \qquad (16)$$

with the boundary conditions $\delta T \rightarrow 0$ at infinity.

An important comment has to be made at this point. The temperature (11) is a symmetric function of x with respect to the sensor position $x = 0$. Therefore, the temperature gradient in (16) is an antisymmetric function. It means that the wire temperature does not change due to the gas flow, in the first order. This is not a problem for the Microflown because there is the other wire at $x = a$ that will feel the presence of the heat flux from the first one. However, it seems to contradict the hot wire anemometry. Actually there is no contradiction. If we would calculate the second-order correction to the temperature it would be defined by the term $-v_0 \partial_x \delta T$, which is symmetric in x. Therefore, for small velocities, the wire temperature changes as v^2. We already stressed that at small gas velocities, the anemometer loses its resolution [15, 21]. It works perfectly well at large Reynolds numbers, $Re \gg 1$, when there is a thin boundary layer around the wire. In that case the heat transfer coefficient is proportional to $\sqrt{Re} \sim \sqrt{v}$ [20]. However, the Microflown operates in the range $Re \ll 1$, where the boundary layer does not exist (formally it is larger than the device size). For this condition, the heat transfer coefficient does not depend on the velocity at all in a first-order approximation [22]. This dependence appears only as $Re^2 \sim v^2$ in full agreement with our conclusion.

Equation (16) is solved using a Fourier transform over the z coordinate

$$\delta\bar{T}(x, q) = \int_{-\infty}^{\infty} \delta T(x, z)\, \mathrm{e}^{\mathrm{i}qz}\, \mathrm{d}z. \qquad (17)$$

The right-hand side of (16) is transformed accordingly, using the stationary temperature distribution (5). For the x dependence of the Fourier amplitude one finds the equation

$$\delta\bar{T}'' - K^2\delta\bar{T} = -\frac{v}{D}\frac{P}{2kl_y}\, \mathrm{sign}(x)\, \mathrm{e}^{-q|x|},$$
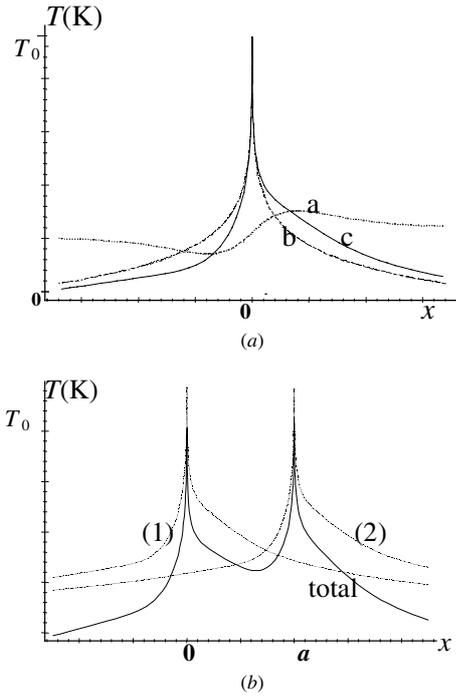$$K = \sqrt{q^2 + \mathrm{i}2\pi f/D}. \qquad (18)$$

Figure 4. (*a*) The original, unperturbed, temperature profile of one heater versus x (b), the perturbation $\delta T(x)$ due to convection (a) and the sum of both (c). (*b*) Temperature due to convection versus x for two heaters at a mutual distance a, as a sum of two single temperature functions.

Here a prime denotes a derivative of x and q should be interpreted as the absolute value $|q|$. The solution of this equation that is continuous at $x = 0$ together with the derivative and decaying at infinity is

$$\delta\bar{T}(x, q) = -\mathrm{i}\frac{v}{2\pi f}\frac{P}{2kl_y}\, \mathrm{sign}(x)(\mathrm{e}^{-q|x|} - \mathrm{e}^{-K|x|}). \qquad (19)$$

It is antisymmetric due to the presence of the sign function.

To find the z dependence of the temperature correction, we have to make the inverse Fourier transform. It is not possible to find it in an analytic form. However, it should be realized that the only place of interest for $\delta T(x, z)$ is at $z = 0$, in which case the inverse transform can be found analytically. If one heater (sensor) is at the position $x = 0$ and the other at $x = a$ then the influence of the first one on the second changes its temperature by $\delta T(a, 0)$. However, the second heater also influences the first one and due to the antisymmetry its temperature changes by $-\delta T(a, 0)$. The device measures this differential temperature. As stated above, the total function for the temperature T consists of two terms of the form (10), e.g. $T_{\text{left heater}}$ and $T_{\text{right heater}}$, with one term shifted over a distance a. The behaviour of $T(x)$ as a sum of two functions is illustrated by figures 4(*a*) and (*b*).

The temperature difference between the wires can be expressed in the form

$$\Delta T = 2\delta T(a, 0) = \mathrm{e}^{\mathrm{i}2\pi f}\frac{2v}{D/a}\frac{P}{2\pi kl_y}\frac{1}{\mathrm{i}\bar{f}}[1 - \sqrt{\mathrm{i}\bar{f}}K_1(\sqrt{\mathrm{i}\bar{f}})], \qquad (20)$$

where $K_1(x)$ is the modified Bessel function of the second kind and the dimensionless frequency was introduced as

$$\bar{f} = \frac{f}{f_D}, \qquad f_D = \frac{D}{2\pi a^2}. \tag{21}$$

Of course, only the real part of ΔT has a physical meaning. The frequency f_D is called the thermal diffusion frequency, which is a characteristic frequency characterizing the frequency behaviour of ΔT. For large $\bar{f}$, the term with the Bessel function decreases exponentially, and the amplitude of ΔT decreases as $1/\bar{f}$. For small $\bar{f}$, i.e. $\bar{f} \ll 1$ or $f \ll f_D$, the behaviour of the Bessel function is

$$\sqrt{i\bar{f}}K_1(\sqrt{i\bar{f}}) = 1 + \frac{i\bar{f}}{2}\left(\ln\frac{\sqrt{i\bar{f}}}{2} + \gamma - \frac{1}{2}\right), \tag{22}$$

and again we are confronted with a divergence problem: ΔT diverges logarithmically in the zero frequency limit. The problem is again connected with the two-dimensional nature of our model. Let us stress that the reason for this divergence is not connected with the finite wire width, which can be safely kept zero; the problem appears due to the small q range (large distances). To avoid the problem, we once again have to return to the real three-dimensional world. As one can see from the expansion (7), there is a smallest wave number along the y direction which is $q_0 = \pi/l_y$. The larger values of n in (7) are not important because they are integrated out in two dimensions but the first one is of principal importance. It is easy to see that to take q_0 into account one has to change q and K (18) into

$$q \rightarrow \sqrt{q_0^2 + q^2}, \qquad K \rightarrow \sqrt{q_0^2 + q^2 + i2\pi f/D}. \tag{23}$$

Then the final expression for the temperature difference can be written as

$$\Delta T = 2\delta T(a,0) = e^{i2\pi f}\frac{2v}{D/a}\frac{P}{2\pi kl_y}\frac{1}{i\bar{f}}$$
$$\times \left[\alpha K_1(\alpha) - \sqrt{\alpha^2 + i\bar{f}}K_1(\sqrt{\alpha^2 + i\bar{f}})\right], \tag{24}$$
$$\alpha = \pi\frac{a}{l_y}.$$

This expression is finite at zero frequency. For small α, the Bessel functions in equation (24) can be expanded in α, and the limit for $f \rightarrow 0$ can be calculated. The difference between the wire temperatures in this case is

$$\Delta T(f=0) = e^{i2\pi f}\frac{2v}{D/a}\frac{P}{4\pi kl_y}(\ln(\pi a/2l_y) + \gamma), \tag{25}$$

where $\gamma = 0.577$ is the Euler constant. It defines the Microflown sensitivity to a constant gas flow. Equation (25) has to be used carefully in applications since it is actually of logarithmic precision and therefore it cannot be very precise. Further, it works only at very low frequencies, which are not too interesting for acoustical applications. Really, as follows from (24), the limit of (25) is true for frequencies

$$f < \frac{\pi D}{4l_y^2},$$

which is about 7 Hz for the current Microflown dimensions.

In the opposite limit we can use equation (20) that is not restricted by the logarithmic precision. Therefore, for the acoustic application formula (20) should work well.

2.3. The effect of the heat capacity of the sensors

The next step in the approach is to take into consideration the heat capacity of the sensors. The effect of this heat capacity becomes important for increasing frequencies. In equation (13), an additional term appears with respect to this effect, so

$$(\rho c_p)_{\text{air}}(\partial_t T + v \cdot \nabla T) + Lh(\rho c_p)_{\text{sensor}}(\delta(x)$$
$$+ \delta(x+a))\delta(z)\partial_t T - \nabla(k\nabla T) = Q. \tag{26}$$

Here h is the thickness of the wire, ρ represents the density and c_p is the heat capacity of the fluid (the air) or the sensor. The sensor consists of a layer of silicon nitride of about 200 nm thickness, and a platinum (or chromium/platinum) wire of ca 100 nm on it. The products ρc_p of both materials are also of the same order of magnitude: $(\rho c_p)_{\text{Pt}} \approx 2.85 \times 10^6$ J m^{-3} K^{-1}; $(\rho c_p)_{\text{SiNi}} \approx 1.66 \times 10^6$ J m^{-3} K^{-1}. This means that in order to calculate the specific value of $h(\rho c_p)_{\text{sensor}}$ in the equation, one should take the sum of both products $h_{\text{Pt}}(\rho c_p)_{\text{Pt}}$ and $h_{\text{SiNi}}(\rho c_p)_{\text{SiNi}}$. For air the similar product is three orders of magnitude smaller $(\rho c_p)_{\text{air}} \approx 1.3 \times 10^3$ J m^{-3} K^{-1}.

If, again, a small perturbation δT is added to this equation, the same approach as to equation (13) leads to

$$\partial_t\delta T - D\nabla^2\delta T = -v\partial_x T$$
$$- Lh\frac{(\rho c_p)_{\text{sensor}}}{(\rho c_p)_{\text{air}}}(\delta(x) + \delta(x-a))\delta(z)\partial_t\delta T, \tag{27}$$

if the two beams of the two-sensor Microflown are at $x=0$ and $x=a$. After the Fourier transform from $\delta T(x,z)$ to $\delta\bar{T}(x,q)$, this can be written as

$$\delta\bar{T}''(x,q) - K^2\delta\bar{T}(x,q) = \frac{v}{D}\partial_x\bar{T}(x,q)$$
$$+ i\frac{f}{f_{hc}}[\delta T(0,0)\delta(x) + \delta T(a,0)\delta(x-a)]. \tag{28}$$

Note that the coefficients near the δ-functions are not the Fourier amplitudes but the original temperature corrections at the wire positions. The second corner frequency f_{hc} has been introduced in (28) as

$$f_{hc} = \frac{D}{2\pi Lh}\frac{(\rho c_p)_{\text{air}}}{(\rho c_p)_{\text{sensor}}} \approx 3000 \text{ Hz}. \tag{29}$$

It is the corner frequency of a first-order low pass filter with which the function $\Delta T(f)$ will be seen to be multiplied when taking the heat capacity into account. The numerical value is given for the room temperature. However, one has to remember that the device operates at quite high temperature and the change of the air density around the wire cannot be neglected. The frequency f_{hc} will be scaled with temperature as the ratio of the room and wire temperatures T_r/T_w.

Equation (28) can be solved in the following way. Consider first one wire located at $x=0$ (no term with $\delta(x-a)$ in (28)). The contribution from the other wire can be added later just shifting the wire position to $x=a$. The term with the δ-function on the right-hand side changes boundary conditions at $x=0$: instead of continuity of the function and its derivative, the δ-function demands a finite discontinuity of the derivative

$$\delta\bar{T}'|_+ - \delta\bar{T}'|_- = i\frac{f}{f_{hc}}\delta T(0,0) \equiv C. \tag{30}$$

1473

The derivative jump C is an unknown constant. One can find the solution of equation (28) expressed via this constant. It is given by the same function (19) plus an additional term:

$$\delta \bar{T}(x,q) = -\mathrm{i}\frac{v}{2\pi f}\frac{P}{2kl_y}\mathrm{sign}(x)(\mathrm{e}^{-q|x|} - \mathrm{e}^{-K|x|}) + \frac{C}{2K}\mathrm{e}^{-K|x|}.$$
(31)

The inverse Fourier transform of this expression at $z = 0$ can be found explicitly

$$\delta T(x,0) = \frac{vx}{D}\frac{P}{2\pi kl_y}\frac{1}{\mathrm{i}\bar{f}_x}$$
$$\times \left[1 - \sqrt{\mathrm{i}\bar{f}_x}K_1\left(\sqrt{\mathrm{i}\bar{f}_x}\right)\right] + \frac{C}{2\pi}K_0\left(\sqrt{\mathrm{i}\bar{f}_x}\right),$$
(32)

$$\bar{f}_x = \frac{2\pi f x^2}{D},$$

where the x-dependent dimensionless frequency f_x has been introduced. It is interesting to note that the δ-term gives a change of the temperature of the wire itself due to the finite heat capacity, so that $\delta T(0,0)$ is no longer zero. Of course, direct application of equation (32) gives an infinite value for $\delta T(0,0)$, but we already know how to deal with it: one has to average first the temperature correction over the wire width and then put $x = 0$. This procedure is equivalent to the change

$$\bar{f}_x(x \to 0) \to \bar{f}_L = 2\pi f L^2/D.$$

To find the unknown constant C and the similar one C' for the jump on the other wire, we have to find the temperature correction produced by both wires $\delta T(x,0) + \delta T(x-a,0)$ and put in it, one by one, $x = 0$ and $x = a$. In the first case the correction will be proportional to C, and in the second case to C'. In this way we will get two linear equations for the unknown constants. The final result for the difference between wire temperatures will be

$$\Delta T = \mathrm{e}^{\mathrm{i}2\pi f}\frac{2v}{D/a}\frac{P}{2\pi kl_y}\frac{1}{\mathrm{i}\bar{f}_a}$$
$$\times \frac{1 - \sqrt{\mathrm{i}\bar{f}_a}K_1\left(\sqrt{\mathrm{i}\bar{f}_a}\right)}{1 - \mathrm{i}\frac{f}{f_{hc}}\left[K_0\left(\sqrt{\mathrm{i}\bar{f}_L}\right) - K_0\left(\sqrt{\mathrm{i}\bar{f}_a}\right)\right]}.$$
(33)

This is the final analytical expression that is proportional to the Microflown sensitivity. The dimensionless frequencies $\bar{f}_a$, $\bar{f}_L$ are defined as $\bar{f}_x$ in (32) for $x = a$ and $x = L$, respectively. Equation (33) differs from (20) only by the dominator, which takes into account the finite heat capacity of the sensors. For small frequencies $f \ll f_{hc}$ (33) coincides with (20) but at higher frequencies it leads to an additional suppression of the sensitivity.

3. Evaluation of the model

The expression for ΔT (equation (33)), that also takes into account the finite heat capacity of the wires, is only slightly different from the antisymmetric function of equation (20). The deviance from pure antisymmetry of the final expression equation (33) is generally only small.

To visualize the temperature of the fluid around the sensors, both the unperturbed and the altered temperature are plotted in figure 4 as a function of x. Note that, due to the fact that the temperature correction is (almost) an antisymmetric function in x, the correction to the temperature at the heater
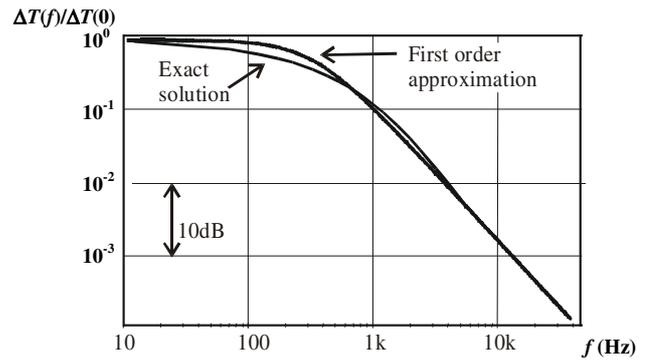
Figure 5. Comparison of the output signal, proportional to ΔT, as calculated from equation (20) to the corresponding first-order function. In equation (20), $a = 300\ \mu$m, $D = 7.7 \times 10^{-5}\ \mathrm{m^2\ s^{-1}}$ at $T = 600$ K due to the temperature dependence of D.

itself is in a first-order approximation zero. Because of this asymmetry, the averaged value over the width of the heater around $x = 0$ is 0; the used perturbation theory predicts *no* change in the temperature at the heater due to flow when there is only one wire.

It is seen that in the situation of two wires (figure 4(*b*)) the temperatures of both heaters *do* change due to the flow; the asymmetry of the function yields a temperature difference between the heaters.

The behaviour of expression (20) for the temperature difference between the wires bears a resemblance to that of a first-order (low pass filter) function. For frequencies small compared to the thermal diffusion frequency f_D, the function is constant (independent of f), for frequencies much higher than this frequency the function is inversely proportional to f; see figure 5. The thermal frequency is an important scale factor in the expression for ΔT, although it does not equal the corner frequency of a corresponding first-order system. For the interpretation of experimentally obtained sensitivity curves, it is useful to fit these curves in an optimization procedure. One approximates then the function (20) by a first-order function $H(f)$ for which $|H(f)| = \frac{\Delta T(0)}{\sqrt{1+(f/f_d)^2}}$, with corner frequency f_d and a magnitude $\Delta T(0)$ at $f = 0$. Frequency f_d differs only by a scale factor from f_D: in defining the dimensionless frequency $f_D = D/2\pi a^2$, only D and a^2 are of real importance, the scale factor in front can be chosen arbitrarily. The theoretical value of $\Delta T(0)$, i.e. the sensitivity for 'steady' flow ($f = 0$) was calculated as in expression (25). In principle, this function can easily be optimized for a to find the optimum mutual wire distance. However, it should be realized that (25) was obtained from an expansion of the Bessel functions in α ($\alpha = a\pi/l_z$), only valid for small α. Differentiating with respect to a and setting equal to zero gives

$$a_{\mathrm{opt}} = \frac{2l_y}{\pi}\mathrm{e}^{-(1+\gamma)} \approx 0.13l_y.$$
(34)

Since this value for a implies that α is almost out of the allowed range, equation (34) can be used only as a crude approximation.

If next the heat capacity of the wires is also taken into account, the total frequency response can be approximated by

$$|\Delta T| = \Delta T(0)\frac{1}{\sqrt{1 + f^2/f_{hc}^2}}\frac{1}{\sqrt{1 + f^2/f_d^2}},$$
(35)

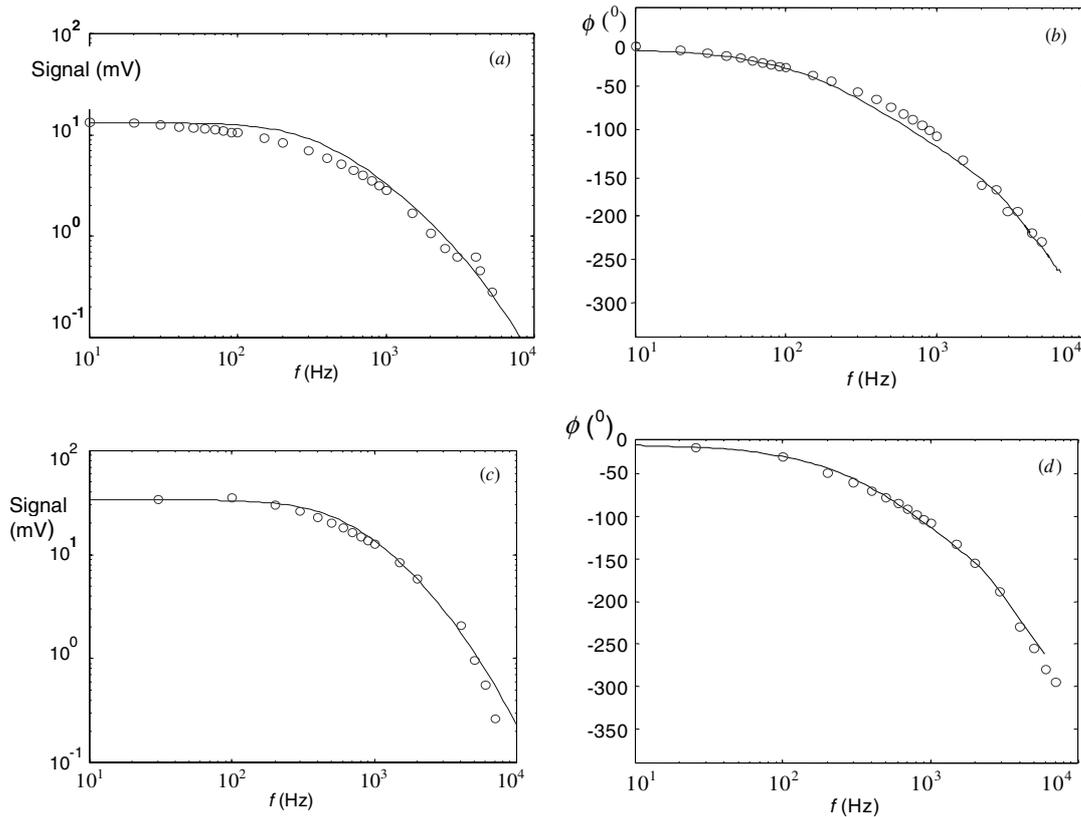**Figure 6.** (a) Magnitude of the experimentally determined sensitivity of a Microflown with $a = 50\ \mu$m, $l = 1$ mm, $L = 2\ \mu$m and $P = 12$ mW (dots), compared to the calculated curve according to equation (33) (line). (b) Phase of the experimentally determined sensitivity of a Microflown with $a = 50\ \mu$m, $l = 1$ mm, $L = 2\ \mu$m and $P = 12$ mW (dots), compared to the calculated curve according to equation (33) (line). (c) Magnitude of the experimentally determined sensitivity of a Microflown with $a = 150\ \mu$m, $l = 1$ mm, $L = 2\ \mu$m and $P = 12$ mW (dots), compared to the calculated curve according to equation (33) (line). (d) Phase of the experimentally determined sensitivity of a Microflown with $a = 150\ \mu$m, $l = 1$ mm, $L = 2\ \mu$m and $P = 12$ mW (dots), compared to the calculated curve according to equation (33) (line).

where f_{hc} is the heat capacity corner frequency. This expression is useful when comparing experimentally obtained sensitivity curves to theory. With the determination of $\Delta T(0)$, f_D and f_{hc} by fitting the measured sensitivity functions of the sensors, the sensors can thus be well characterized for typical operation conditions.

4. Comparison to experimental results

For an experimental investigation of the sensitivity of various sensors, Microflowns of varying mutual wire distance a, width L and length l_y were designed. Having designed first the different masks for the required wafers, we started the process with the deposition of a 200 nm thick layer of silicon nitride on which an adhesion layer of 10 nm chromium and a 90 nm thick platinum layer was deposited by sputtering. Then it was patterned by lift off. Subsequently the silicon nitride was etched by reactive ion etching (RIE) followed by anisotropic etching in KOH to etch the beams free. This underetching was achieved by a slight misalignment of the mask (see also [1]).

The measurements of the Microflowns were performed in a 'standing wave tube'. This is a long tube with a sound source generating a broad frequency spectrum at one side, and a reflecting cross section with a reference microphone in it at the other side. In the tube standing wave patterns occur.

Somewhere along this standing wave tube a Microflown is placed, so that from the ratio between the signals of the reference microphone and the Microflown the sensitivity of the latter can be deduced [1, 8, 11]. For frequencies above 4 kHz, up to about 20 kHz, both sensors have to be utilized in an anechoic room, since the standing wave tube can no longer be used for frequencies higher than, depending on its precise geometry, a few kHz. In these experiments the sensitivity was measured as a function of frequency for frequencies in the spectrum of $0 < f < 4.0 \times 10^3$ Hz.

For an investigation of the mutual variance in sensitivity of sensors of the same geometry, and the errors due to the measurement set-up, first several sensors of exactly the same geometry were successively measured. From these results it could be concluded that the compound reproducibility of measurements and fabrication technology was better than 2%.

The parameters to be varied in the experiments were chosen to be the following dimensions of the sensor: the width L, the mutual wire distance a and the wire length l_y. The dimensions were varied independently.

Comparing Microflowns with wire lengths of 0.5; 1.0; 1.5 and 3.0 mm showed that l_y is not of significant influence on the sensitivity, which is in accordance with what is theoretically expected.

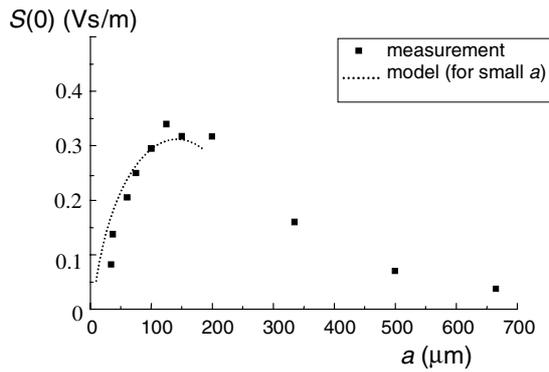Next, the influence of the mutual wire distance a on the low frequency sensitivity and the characteristic frequency f_d

Figure 7. Magnitude of the low frequency sensitivity (determined from the output signal at ca 10 Hz), as a function of mutual wire distance a. Dissipated power $P = 16$ mW, $l_y = 1$ mm. The calculated value of $S(0)$ according to equation (25), valid for small a, is shown by the dotted line.

Figure 8. The corner frequency f_{hc} due to the heat capacity, as a function of the inverse of the wire width, L^{-1}. The line shows the calculated value for a 200 nm thick silicon nitride beam with a 100 nm thick platinum layer of 1 mm length.

Figure 9. Characteristic frequency f_d of the fitted sensitivity curves, as a function of the distance between the sensing wires, plotted logarithmically. The line shows the theoretical dependence $f_d \propto a^{-2}$.

was investigated. Therefore, different sensors, with a varying from 30, 60, 90, ... to 700 μm have been measured in the standing wave tube. From the ratio of the output signal and the sensitivity of the reference microphone, the sensitivity curves were obtained. These were compared to the model calculations of the sensitivity for the concerned parameter values, equation (33). Two representative results for both magnitude and phase of the sensitivity, for wire separations $a = 50$ μm and $a = 150$ μm, are shown in figure 6. The theoretical curves are depicted by the lines; these are obtained from the explicit calculation of expressions (33) and (1).

The temperature coefficient of the resistance, θ, (equation (1)), was measured to be 3.0×10^{-3} K^{-1}. The applied voltage by the source was $U_0 = 10$ V. For each geometry, the output signal u_0 as a function of frequency, and f_d and f_{hc} were calculated. It is seen that the experimentally obtained points and the calculated curves correspond rather well, without any fitting parameters.

The measured output voltage functions of all sensors were approximated by the product of two 'first-order' functions, equation (35) to find $\Delta T(0)$, f_d and f_{hc}. In figure 7, the low frequency sensitivity $S(0)$, the output voltage per m s^{-1}, is plotted as a function of a. For comparison, the calculated value according to equations (25) and (1) is also depicted. As stated before, the deduced expression (25) is only an approximation, and only valid for $\pi a / l_y$ small. However, the calculated optimum $a_{\text{opt}} = 130$ μm is in satisfactory correspondence with the experimental results.

The wire width L and separation a of the various sensors were independently varied. From the approximations of the measured sensitivity functions, the two corner frequencies could thus be obtained. A very precise determination of the first characteristic frequency f_d becomes difficult for small a (so that f_d becomes large, above ca 5 kHz), since the other corner frequency $f_{hc} \approx 3$ kHz (for $L = 2$ μm) then dominates the sensitivity function. For f_d and f_{hc} of about the same magnitude, both values cannot very well be discriminated. The heat capacity corner frequency is inversely proportional to the thermal mass of the sensor (equation (29)), that is $f_{hc} \sim L^{-1}$. The experimentally obtained corner frequencies f_{hc} are shown in figure 8 as a function of the inverse of the wire width, together with the theoretical proportionality. The
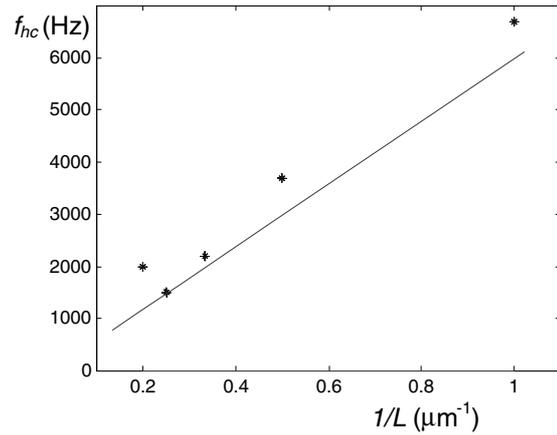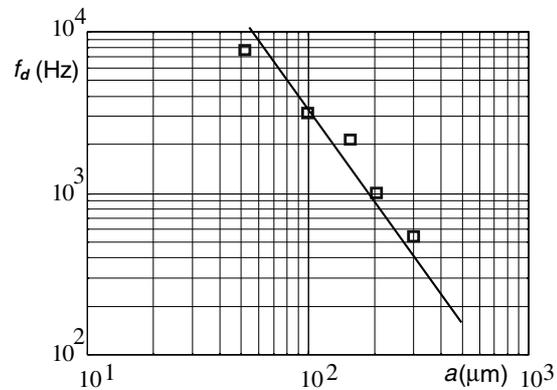
theoretical line is calculated for the used material parameters and dimensions of the sensor wire. For $L = 2$ μm, a value of $f_{hc} \approx 3.6$ kHz was found, which is not too far from the calculated value $f_{hc} \approx 3$ kHz (equation (29)) for this geometry.

Next, in figure 9 the corner frequencies f_d are depicted. As can be expected from equation (21), f_d should be proportional to a^{-2}, whose line is also shown. Due to the difficulty in distinguishing two separate, different, first-order functions the errors in f_{hc} and f_d can be relatively large for some fits. The correspondence between theory and experiment seems nevertheless sufficient, for both corner frequencies.

5. Conclusions and future research

For a reliable description of the behaviour of the Microflown, and to deduce an expression for the sensitivity of the flow sensor as a function of frequency, geometrical and material parameters, an analytical model was developed. This was done by a calculation of the temperature distribution around the two heated wires and the perturbation due to the forced convection by an acoustic wave. It was seen that the wires' resulting

temperature difference can be calculated using perturbation theory. The frequency-dependent behaviour of the output signal was thus analysed. In the sensitivity function, two important characteristic frequencies are found. The shape of the function is mainly determined by the first characteristic frequency; the 'thermal frequency'. It is proportional to the quotient D/a^2, with D being the heat diffusion coefficient of the fluid (generally the air) and a being the mutual distance between the wires. The dependence of the first characteristic frequency on a, namely $f_d \sim a^{-2}$, has been verified in experiments. The experimentally obtained values of this characteristic frequency are found to be in satisfactory correspondence to the model.

Second, the heat capacity of the heaters causes an additional 'first-order' frequency dependence. The corresponding corner frequency depends on D, the geometry of the heated wires and of course on the thermal masses of the sensor material and the fluid.

For the heaters used in the experiment, the theoretical value of this corner frequency can be calculated as $f_{hc} = 3\,\mathrm{kHz}$ for $L = 2\,\mu\mathrm{m}$. Both the experimentally found magnitude and the dependence on the wire width of the corner frequency f_{hc} are in acceptable agreement with the theory.

Another very important parameter of the sensitivity function is its magnitude for steady ('dc') flows, $S(0)$. From the developed theory this value can be calculated explicitly, although the deduced expression is an approximation and valid only for small a. The dependence of $S(0)$ on a and also the thus calculated optimum a_{opt} are experimentally confirmed.

Concluding, all characteristic parameters of the frequency-dependent sensitivity of the Microflown, found in measurements, correspond both qualitatively and quantitatively well to the model; the developed analysis was confirmed by experimental results and provides a reliable description. In future work, this model can be used as a starting point for further optimization of the sensor, with regard to frequency range and signal-to-noise ratio for specific applications. Besides, the theory appears to be applicable even for other geometries, such as three-wire configurations. These future devices, with improved dimensions, have to be investigated both theoretically and experimentally.

Acknowledgments

References

[1] de Bree H-E *et al* 1996 The Microflown: a novel device measuring acoustical flows *Sensors Actuators* A **54** 552–7

[2] de Bree H-E, Lammerink T S J, Elwenspoek M C and Fluitman J H J 1995 Use of a fluid flow measuring device as a microphone and system comprising such a microphone *Patent* PCT/NL95/00220

[3] Druyvesteyn W F *et al* 2000 A new sound intensity probe; comparison to the Bruel & Kjaer p-p probe *J. Audio Eng. Soc.* **48** 49–56

[4] Druyvesteyn W F *et al* 1999 *A New Acoustic Measurement Probe; The Microflown* (London: IOA)

[5] de Bree H-E *et al* 1999 Three-dimensional sound intensity measurements using microflown particle velocity sensors *MEMS'99 (Orlando)*

[6] de Bree H-E *et al* 1999 Realisation and calibration of a novel half inch p-u sound intensity probe *106th AES (Munchen)*

[7] Schurer H *et al* 1996 Comparison of two methods for measurement of horn input impedance *Proc. 100th AES Convention (Copenhagen)*

[8] van der Eerden F J M *et al* 1998 Experiments with a new acoustic particle velocity sensor in an impedance tube *Sensors Actuators* A **69** 126–33

[9] de Bree H E *et al* 1996 A method to measure apparent acoustic pressure, Flow gradient and acoustic intensity using two micro machined flow microphones *Eurosensors X (Leuven)*

[10] de Bree H-E *et al* 1999 Bi-directional fast flow sensor with a large dynamic range *J. Micromech. Microeng.* **9** 186–9

[11] Druyvesteyn W F *et al* 1998 Intensity measurements in various rooms/a new intensity probe *16th ICA and 135th ASA Meeting (Seattle June 1998)* vol 4 pp 2827–8

[12] Svetovoy V B and Winter I A 2000 Model of the μ-flown microphone *Sensors Actuators* **86** 171–81

[13] Spiegel M R 1974 *Advanced Calculus* (New York: McGraw-Hill)

[14] de Bree H E 2000 Add-on Microflown for a high-end pressure gradient microphone *Proc. 109th AES Convention (Los Angeles)* no 5181

[15] Lomas C G 1986 *Fundamentals of Hot Wire Anemometry* (Cambridge: Cambridge University Press)

[16] Johnson R G *et al* 1987 A highly sensitive silicon chip microtransducer for air flow and differential pressure applications *Sensors Actuators* **11** 63–72

[17] Yang C and Søeberg H 1992 Monolithic flow sensor for measuring milliliter per minute flow *Sensors Actuators* A **33** 143–53

[18] Petersen K *et al* 1985 High precision, high performance mass-flow sensor with integrated laminar flow micro-channels *Sensors Actuators* **7** 361–3

[19] Hocker G B 1985 A microtransducer for air flow and differential pressure sensing applications *Micromachining and Micropackaging of Transducers* pp 207–14

[20] King L V 1914 On the convection of heat from small cylinders in a stream of fluid (esp. Determination of the convection constants of small platinum wires with application to hot wire anemometry) *Proc. R. Soc.* A **90** 563, 373

[21] Kohl F, Jachimowicz A, Steurer J, Glatz R, Kuttner J, Biacovsky D, Olcaytug F and Urban G 1994 A micromachined flow sensor for liquid and gaseous fluids *Sensors Actuators* A **41** 293–9

[22] Landau L D 1987 *Fluid Mechanics* (*Course of Theoretical Physics* vol 6) ed L D Landau and E M Lifschitz

[23] De Bree H-E 2001 *The Microflown* (Amsterdam, The Netherlands)

[24] www.processcontrolscorp.com/thermal.htm; www.kurz-instruments.com/a6.pdf

[25] Holman J P 2002 *Heat Transfer* 9th edn (MacGregor and Emery)